THE HST KEY PROJECT ON THE EXTRAGALACTIC DISTANCE SCALE. XV. IMPLICATIONS OF A CEPHEID DISTANCE TO THE FORNAX CLUSTER

BARRY F. MADORE[1], WENDY L. FREEDMAN[2], N. SILBERMANN[3]

PAUL HARDING[4], JOHN HUCHRA[5], JEREMY R. MOULD[6]

JOHN A. GRAHAM[7], LAURA FERRARESE[8]

BRAD K. GIBSON[5], MINGSHENG HAN[9], JOHN G. HOESSEL[9]

SHAUN M. HUGHES[10], GARTH D. ILLINGWORTH[11]

RANDY PHELPS[2], SHOKO SAKAI[3], PETER STETSON[12]

---

1 NASA/IPAC Extragalactic Database, Infrared Processing and Analysis Center, Jet Propulsion Laboratory, California Institute of Technology, MS 100-22, Pasadena, CA 91125

2 Observatories of the Carnegie Institution of Washington, 813 Santa Barbara St., Pasadena, CA 91101

3 Jet Propulsion Laboratory, California Institute of Technology, MS 100-22, Pasadena, CA 91125

4 Steward Observatory, University of Arizona, Tucson, AZ 85721

5 Harvard Smithsonian Center for Astrophysics, 60 Garden Street, Cambridge, MA 02138

6 Mt. Stromlo and Siding Spring Observatories, Institute of Advanced Studies, Private Bag, Weston Creek Post Office, ACT 2611, Australia

7 Department of Terrestrial Magnetism, Carnegie Institution of Washington, 5241 Broad Branch Rd. N.W., Washington D.C. 20015

8 Hubble Felow, California Institute of Technology, MS 105-24 Robinson Lab, Pasadena, CA 91125

9 Department of Astronomy, University of Wisconsin, 475 N. Charter St., Madison, WI 53706

10 Royal Greenwich Observatory, Madingley Road, Cambridge, UK CB3 OHA

11 Lick Observatory, University of California, Santa Cruz, CA 95064

† † † Dominion Astrophysical Observatory, 5071 W. Saanich Rd., Victoria, BC, Canada V8X 4M6

ABSTRACT

Using the Hubble Space Telescope (HST) thirty-seven long-period Cepheid variables have been discovered in the Fornax Cluster spiral galaxy NGC 1365 (Silbermann et al. 1998). The resulting V and I period-luminosity relations yield a true distance modulus of $\mu_o = 31.35 \pm 0.07$ mag, which corresponds to a distance of 18.6±0.6 Mpc. This measurement provides several routes for estimating the Hubble Constant. (1) Assuming this distance for the Fornax Cluster as a whole yields a local Hubble Constant of 70 $(\pm 7)_{\rm random}$ $[\pm 18]_{\rm systematic}$ km/s/Mpc. (2) Nine Cepheid-based distances to groups of galaxies out to and including the Fornax and Virgo clusters yield $H_o = 73$ $(\pm 4)_r$ $[\pm 17]_s$ km/s/Mpc. (3) Recalibrating the I-band Tully-Fisher relation using NGC 1365 and six nearby spiral galaxies, and applying it to 15 galaxy clusters out to 100 Mpc gives $H_o = 76$ $(\pm 2)_r$ $[\pm 8]_s$ km/s/Mpc. Fourth, using a broad-based set of differential cluster distance moduli ranging from Fornax to Abell 2147 gives $H_o = 72$ $(\pm 1)_r$ $[\pm 7]_s$ km/s/Mpc. And finally (4) Assuming the NGC 1365 distance for the two additional Type Ia supernovae in Fornax and adding them to the SnIa calibration (correcting for light curve shape) gives $H_o = 67$ $(\pm 5)_r$ $[\pm 8]_s$ km/s/Mpc out to a distance in excess of 500 Mpc. All five of these H_o determinations agree to within their statistical errors. The resulting estimate of the Hubble Constant combining all these determinations is $H_o = 72$ $(\pm 5)_r$ $[\pm 12]_s$ km/s/Mpc.

1. INTRODUCTION

Hubble (1929) announced his discovery of the expansion of the Universe nearly 70 years ago. Despite decades of effort, and continued improvements in the actual measurement of extragalactic distances, convergence on a consistent value for the absolute expansion rate, the Hubble constant, H_o, has been elusive. However, progress on the absolute calibration of the extragalactic distance scale in the last few years has been rapid and dramatic (see, the recent proceedings *"The Extragalactic Distance Scale"* edited by Livio, Donahue & Panagia 1997 for instance, containing Freedman, Madore & Kennicutt 1997; Mould et al. 1997; Tammann & Federspiel 1997; and also see Jacoby et al. (1992) and Riess, Press & Kirshner 1996). This accelerated pace has occurred primarily as a result of the improved resolution of the Hubble Space Telescope (HST) and its consequent ability to discover classical Cepheid variables at distances a factor of ten further than can routinely be achieved from the ground. As a result, accurate zero points to a number of recently refined methods which can measure precise relative distances beyond the realm of the Cepheids have become available. These combined efforts are providing a more accurate distance scale for local galaxies, and are indicating a convergence among various secondary distance indicators in establishing an absolute calibration of the far-field Hubble flow.

The discovery of Cepheids with HST has proven to be very efficient out to and even somewhat beyond distances of ~20 Mpc. Soon after the December 1993 HST servicing mission the measurement of Cepheids in the Virgo cluster (part of the original design specifications for the telescope) became feasible (Freedman et al. 1994a). The subsequent discovery of Cepheids in the Virgo galaxy M100 (Freedman et al. 1994b; Ferrarese et al. 1996) were important steps in resolving outstanding differences in the extragalactic distance scale (Mould et al. 1995). The Virgo cluster is complex both in its geometric and its kinematic structure, and there still remain large uncertainties in both the velocity and distance to this cluster. Hence, the Virgo cluster is not an ideal test site for an unambiguous determination of the cosmological expansion rate or the

calibration of secondary distance indicators. In this paper we discuss the implications of a Cepheid distance to the next major cluster of galaxies, Fornax, which is a much simpler system than Virgo.

In the companion paper to this one (Silbermann et al. 1998) we present the Cepheid photometry and PL relations for the Cepheids in NGC 1365. In Madore et al. (1998) we briefly discussed the determination of H_o based on the distance of NGC 1365 and the Fornax Cluster, in addition to a calibration of a local Hubble expansion-rate plot. The Fornax cluster is comparable in distance to the Virgo cluster (de Vaucouleurs 1975), but it is found almost opposite to Virgo in the skies of the southern hemisphere. The Fornax cluster is less rich in galaxies than Virgo (Ferguson & Sandage 1988), but it is also substantially more compact than its northern counterpart (Figure 1). As a result of its lower mass, the influence of Fornax on the local velocity field is less dramatic than that of the Virgo cluster. And because of its compact nature, questions concerning the membership and location in the cluster of individual galaxies are significantly less problematic; the back-to-front geometry is far simpler and less controversial than that of the Virgo cluster. Clearly, Fornax is a much more interesting site for a test of the local expansion rate.

In the context of the Key Project on the Extragalactic Distance Scale (Kennicutt, Freedman & Mould 1995), there are several important reasons to secure a distance to the Fornax cluster. The Fornax cluster serves as both a probe of the local velocity field and a major jumping-off point for several secondary distance indicators, which can be used to probe a volume of space at least 1,000 times larger. To obtain a distance to the Fornax cluster, the Key Project is configured to monitor three member galaxies; the first of these, discussed here, is the Seyfert 1 galaxy NGC 1365, a striking, two-armed, barred-spiral galaxy with an active galactic nucleus. Two additional galaxies, NGC 1425 and NGC 1326A, have now also been imaged with HST and those data are being processed.

At least three lines of evidence independently suggest that NGC 1365 is a representative, physical member of the Fornax cluster. First, NGC 1365 is almost directly along our line of sight

to Fornax: the galaxy is projected only ~70 arcmin from the geometric center of the cluster, whereas the diameter of the cluster is at least 200 arcmin (Ferguson 1989; see also Figure 1). In addition, NGC 1365 is also coincident with the Fornax cluster in velocity space. The observed velocity of NGC 1365 (+1,636 km/sec) is only +234 km/sec larger than the cluster mean, and is well inside the cluster velocity dispersion (see below.) Finally, we note that for its rotational velocity, NGC 1365 sits within 0.02 mag of the central ridge line of the apparent Tully-Fisher relation relative to other cluster members defined by recent studies of the Fornax cluster (Bureau, Mould & Staveley-Smith 1996; Schroder 1995).

NGC 1365 is large in angular size, and it is very bright in apparent luminosity as compared to any other galaxy in the immediate vicinity of the Fornax cluster. One might question whether on this basis, NGC 1365 is a true member of the Fornax cluster. Correcting for an inclination of 44°, the 21cm neutral hydrogen line width of NGC 1365 is found to be ~575 km/sec (Bureau et al. 1996; Mathewson, Ford & Buchhorn 1992). Using the Tully-Fisher relation as a *relative* guide to intrinsic size and luminosity, this rotation rate places NGC 1365 among the most luminous galaxies in the local Universe; brighter than M31 or M81, and comparable to NGC 4501 in the Virgo cluster or NGC 3992 in the Ursa Major cluster. Thus, the Tully-Fisher relation predicts that NGC 1365 is expected to be apparently bright, even at the distance of the Fornax cluster, and that its observed global properties are consistent with membership in that cluster.

2. THE MEAN VELOCITY AND VELOCITY DISPERSION OF FORNAX

The systemic (heliocentric) velocity and velocity dispersion of the main population of galaxies in Fornax are well defined. A search of the NASA/IPAC Extragalactic Database (NED: http://nedwww.ipac.caltech.edu, Version release date 01/98) for galaxies within 6° of the Fornax cluster center and having published redshifts $\leq$2,500 km/sec produced a sample of 106 galaxies; this was was then supplemented with 4 additional redshifts from ZCAT, (Huchra, Geller, Clemens, Tokarz & Michel 1992; the 1998 edition of ZCAT is available via anonymous ftp from fang.harvard.edu.) and 7 recently published dwarf galaxy redshifts from Drinkwater & Gregg (1998), giving a total of 117 redshifts. Their distribution projected on the sky is shown in Figure 2; and two 'pie diagrams' illustrating the sample distribution in position-velocity space are shown in Figure 3. In all three representations, ellipticals are shown as filled circles, spirals as open circles. While the core of the cluster is demonstrably dominated by E/S0 galaxies, there is no other obvious segregation of the two populations: spirals and ellipticals being coincident and largely co-spatial. After subdividing the sample by morphological type, 39 spirals/irregular galaxies give V = 1,399 km/sec and $\sigma = \pm$334 km/sec, 78 E/SO galaxies give V = 1,463 km/sec with $\sigma = \pm$347 km/sec. The mean velocity of the spirals agrees with the mean for the ellipticals to within 0.2 $\times\sigma$, the velocity dispersion of the system. The combined sample of 117 galaxies has an unweighted mean of V = 1,441 km/sec and $\sigma = \pm$342 km/sec which we adopt hereafter (see also Schroder 1995; Han & Mould 1990.) The velocity off-set of +195 km/sec for NGC 1365 with respect to this mean is less than 2/3 of the cluster velocity dispersion. [1]

[1] Given that the redshifts are of mixed quality with regard to reported uncertainties, differing by up to two orders of magnitude, we also calculated the systemic velocity of the cluster weighting the individual velocities by the inverse square of the internal errors. That solution gives V = 1,405 km/sec, agreeing with the adopted value to within 3%, despite the fact that it is heavily weighted by only a dozen or so high precision points in the distribution (see Figure 4).

3. HST OBSERVATIONS AND THE CEPHEIDS IN NGC 1365

Using the *Wide Field and Planetary Camera 2* on HST, we have obtained a set of 12-epoch observations of NGC 1365. The observing window of 44 days, beginning August 6, and continuing until September 24, 1995, was selected to maximize target visibility, without necessitating any roll of the targeted field of view. Sampling within the window was prescribed by a power-law distribution, tailored to optimally cover the light and color curves of Cepheids with anticipated periods in the range 10 to 60 days (see (3) for additional details). Contiguous with 4 of the 12 V-band epochs (5,100 sec each through the F555W filter), I-band exposures (5,400 sec each through the F814W filter) were also obtained so as to allow a determination of reddening corrections for the Cepheids.

All frames were pipeline pre-processed at the *Space Telescope Science Institute* in Baltimore and subsequently analyzed using two stellar photometry packages, ALLFRAME (Stetson 1994) and DoPhot (Schecter et al. 1993), in order to quantify potential systematic differences in the two reduction programs. Zero-point calibrations for the photometry were adopted from Holtzmann, J. et al. (1995) and Hill et al. (1998), which agree to 0.05 mag on average. Details on the DoPhot and ALLFRAME reduction and analysis of this data set are presented elsewhere (Silbermann et al. 1998). We are also currently undertaking artificial star tests on these frames to quantify the uncertainty due to crowding (Ferrarese et al., in preparation).

Detailed information on the 52 Cepheid candidates discovered in NGC 1365 can be found in Silbermann et al. (1998). The phase coverage in all cases is sufficiently dense and uniform that the form of the light curves is clearly delineated. This allowed 37 of these variables to be unambiguously classified as high-quality Cepheids on the basis of their distinctively rapid brightening, followed by a long linear decline phase (for both the DoPhot and ALLFRAME variable-star candidates). Periods, obtained using a modified Lafler-Kinman algorithm (Lafler & Kinman 1965), are statistically good to a few percent, although in some cases ambiguities larger than this do exist as a consequence of

the narrow observing window and the restricted number of cycles (between 1 and 5) covered within the 44-day window.

The resulting V and I period-luminosity relations for the select set of 37 Cepheids (using intensity-averaged magnitudes) are shown in the upper and lower panels of Figure 5, respectively. The derived apparent moduli are $\mu_V = 31.68\pm(0.05)_r$ mag and $\mu_I = 31.55\pm(0.05)_r$ mag. Correcting for a derived total line-of-sight reddening of $E(V-I)_{N1365} = 0.14$ mag (derived from the Cepheids themselves) gives a true distance modulus of $\mu_0 = 31.35\pm(0.07)_r$ mag. This corresponds to a distance to NGC 1365 of $18.6\pm(0.6)_r$ Mpc, which is within 2% of the value derived from phase-weighted magnitudes as given in Silbermann et al. (1998). The quoted error at this step in the discussion quantifies only the statistical (random) uncertainty generated by photometric errors in the ALLFRAME data combined with the intrinsic magnitude and color width of the Cepheid instability strip.

4. THE HUBBLE CONSTANT

We now discuss the impact of a Cepheid distance to the Fornax cluster in estimating the Hubble constant. Below we present and discuss three independent estimates, where the analysis is based both on the new Fornax distance and the distances to other Key Project galaxies, consistently scaled to a true distance of 18.50 mag for the Large Magellanic Cloud. At the end we intercompare the results for convergence and consistency. The first estimate is based solely on the Fornax cluster, its velocity and the Cepheid-based distance to one of its members. It samples the flow in one particular direction at a distance of ~20 Mpc. We then examine the inner volume of space, leading up to and including both the Virgo and Fornax clusters. This has the added advantage of averaging over different samples and a variety of directions, but it is still limited in volume (to an average distance of ~10 Mpc), and it is subject to the usual caveats concerning bulk flows and the adopted Virgocentric flow model (Table 1). The third estimate comes from using the Cepheid distance to Fornax to lock into secondary distance indicators, thereby allowing us to step

out to cosmologically significant velocities (10,000 km/sec and beyond) corresponding to distances greater than 100 Mpc. Averaging over the sky, and working at large redshifts, alleviates the flow problems. Examining consistency between the independent secondary distance estimates, and then averaging over their far-field estimates should provide a systematically secure value of H_o and, more importantly, a measure of its external error. Comparison of the three 'regional' estimates (Fornax, local and far-field) then can be used to provide a check on the systematics resulting from the various assumptions made independently at each step.

5. UNCERTAINTIES IN THE FORNAX CLUSTER DISTANCE AND VELOCITY

The two panels of Figure 1 show a comparison of the Virgo and Fornax clusters of galaxies drawn to scale, as seen projected on the sky. The comparison of apparent sizes is appropriate given that the two clusters are at approximately the same distance from us. In the extensive Virgo cluster (right panel), the galaxy M100 can be seen marked $\sim 4°$ to the north-west of the elliptical-galaxy-rich core; this corresponds to an impact parameter of 1.3 Mpc, or 8% of the distance from the LG to the Virgo cluster. The Fornax cluster (left panel) is more centrally concentrated than Virgo, so that the back-to-front uncertainty associated with its three-dimensional spatial extent is reduced for any randomly selected member. Roughly speaking, converting the total angular extent of the cluster on the sky ($\sim 3°$ in diameter; Ferguson & Sandage 1988) into a back-to-front extent, the error associated with any randomly chosen galaxy in the Fornax cluster, translates into a few percent uncertainty in distance; this uncertainty in distance will soon be reduced when the two additional Fornax spirals are observed with HST in the coming year.

Here, we note that the infall-velocity correction for the Local Group motion with respect to the Virgo cluster (and its associated uncertainty) becomes a minor issue for the Fornax cluster. This is the result of a fortuitous combination of geometry and kinematics. We now have Cepheid distances from the Local Group to both the Fornax and Virgo clusters. Combined with their angular separation on the sky, this immediately leads to the physical separation between the two clusters.

Under the assumption that the Virgo cluster dominates the local velocity perturbation field at the Local Group **and** at Fornax, we can calculate the velocity perturbation at Fornax (assuming that the flow field amplitude scales with $1/R_{Virgo}$ and characterized by a R^{-2} density distribution, Schechter 1980). From this we then derive the flow contribution to the measured line-of-sight radial velocity, as seen from the Local Group. Figure 6 shows the distance scale structure (left panel) and the velocity-field geometry (right panel) of the Local Group–Virgo–Fornax system. An infall velocity of the Local Group toward Virgo of +200 km/sec is obtained by minimizing the velocity residuals for the galaxies with Cepheid-based distances. This value is in good agreement with that estimated by Han & Mould (1990). We adopt 200±100 km/sec, which results in a projected Virgocentric flow correction for Fornax of −45±23 km/sec.

6. H_o AT FORNAX, AND ITS UNCERTAINTIES

Correcting to the barycentre of the Local Group (−90 km/sec) and compensating for the −45 km/sec component of the Virgocentric flow derived above, we calculate that the cosmological expansion velocity of Fornax is 1,306 km/sec. Using our Cepheid distance of 18.6 Mpc for Fornax gives $H_o = 70\ (\pm 7)_r\ [\pm 18]_s$ km/sec/Mpc. The first uncertainty (in parentheses) includes random errors in the distance derived from the PL fit to the Cepheid data, as well as random velocity errors in the adopted Virgocentric flow, combined with the distance uncertainties to Virgo propagated through the flow model. The second uncertainty (in square brackets) quantifies the currently identifiable systematic errors associated with the adopted mean velocity of Fornax, and the adopted zero point of the PL relation (combining in quadrature the LMC distance error, a measure of the metallicity uncertainty, and a conservative estimate of the stellar photometry errors). Finally, we note that according to the Han-Mould model (Han & Mould 1990), the so-called "Local Anomaly" gives the Local Group an extra velocity component of approximately +73 km/sec towards Fornax. If we were to add that correction our local estimate, the Hubble constant would increase to H_o = 74 km/sec/Mpc.

Given the highly clumped nature of the local universe and the existence of large-scale streaming velocities, there is still a lingering uncertainty about the total peculiar motion of the Fornax cluster with respect to the cosmic microwave background restframe. Observations of flows, and the determination of the absolute motion of the Milky Way with respect to the background radiation suggest that line-of sight velocities ~300 km/sec are not uncommon (*e.g.* Coles & Lucchin 1995 and references therein). The uncertainty in absolute motion of Fornax with respect to the Local Group then becomes the largest outstanding uncertainty at this point in our error analysis: a 300 km/sec flow velocity for Fornax would result in a systematic error in the Hubble constant of ~20%. We can revisit this issue, however, following an analysis of more distant galaxies made later in this section.

7. THE NEARBY FLOW FIELD

We now step back somewhat and investigate the Hubble flow between us and Fornax, derived from galaxies and groups of galaxies inside 20 Mpc, each having Cepheid-based distances and expansion velocities individually corrected for a Virgocentric flow model (see Kraan-Korteweg 1986, for example). These data are presented in Figure 7. At 3 Mpc the M81-NGC 2403 Group (for which both galaxies of this pair have Cepheid distance determinations) gives H_o = 75 km/sec/Mpc after averaging their two velocities. Working further out to M101, the NGC 1023 Group and the Leo Group, the calculated values of H_o range from 62 to 99 km/sec/Mpc. An average of these independent determinations including Virgo and Fornax, gives $H_o = 73\ (\pm 4)_r$ km/sec/Mpc. This determination, as before, uses a Virgocentric flow model with a $1/R_{Virgo}$ infall velocity fall-off, scaled to a Local Group infall velocity of +200 km/sec.

The foregoing determination of H_o is again predicated on the assumption that the infall flow-corrected velocities of both Fornax and Virgo are not further perturbed by other mass concentrations or large-scale flows, and that the 25,000 Mpc^3 volume of space delineated by them is at rest with respect to the distant galaxy frame. To avoid these local uncertainties we now step out from Fornax to the distant flow field. There we explore three applications: (i) Use of the

Tully-Fisher relation calibrated by Cepheids locally, and now including NGC 1365 and about two dozen additional galaxies in the Fornax cluster. Ultimately these calibrators are tied into the distant flow field at 10,000 km/sec defined by the the Tully-Fisher sample of galaxies in clusters (Aaronson et al. 1980; Han 1992). (ii) Using the distance to Fornax to tie into averages over previously published differential moduli for independently selected distant-field clusters, (iii) Recalibrating the Type Ia supernova luminosities at maximum light, and applying that calibration to events as distant as 30,000 km/sec.

8. BEYOND FORNAX: THE TULLY-FISHER RELATION

Quite independent of its association with the Fornax cluster as a whole, NGC 1365 provides an important calibration point for the Tully-Fisher relation which links the (distance-independent) peak rotation rate of a galaxy to its intrinsic luminosity. In the left panel of Figure 8 we show NGC 1365 (in addition to NGC 925 (Silbermann et al. 1996), NGC 4536 (Saha et al. 1996) and NGC 4639 (Sandage et al. 1996) added to the ensemble of calibrators having published Cepheid distances from ground-based data (Freedman 1990), and I-band magnitudes (Pierce 1994 and references therein). As mentioned earlier NGC 1365 provides the brightest data point in the relation; additional galaxies recently added include NGC 3621 (Rawson 1997), NGC 3351 (Graham 1997) and NGC 2090 (Phelps 1998), and will be included once I-band magnitudes become available.

Although we have only the Fornax cluster for comparison at the present time, it is interesting to note that there is no obvious discrepancy in the Tully-Fisher relation between galaxies in the (low-density) field and galaxies in this (high-density) cluster environment. The NGC 1365 data point is consistent with the data for other Cepheid calibrators. Adding in all of the other Fornax galaxies for which there are published I-band magnitudes and inclination-corrected HI line widths provides us with another comparison of field and cluster spirals. In the right panel of Figure 8 we see that the 21 Fornax galaxies (shifted by the true modulus of NGC 1365) agree extremely well with the 9 brightest Cepheid-based calibrators. The slope of the relation is virtually unchanged by this

augmentation; with the scatter about the fitted line increasing somewhat to ±0.35 mag (nevertheless the small intrinsic scatter in the relation greatly diminishes the impact of Malmquist-bias.) In following applications we adopt $M_I = -8.80\ (\log(\Delta V) - 2.445) + 20.47$ as the best-fitting least squares solution for the calibrating galaxies.

Han (1992) has presented I-band photometry and neutral-hydrogen line widths for the determination of Tully-Fisher distances to individual galaxies in 16 clusters out to redshifts exceeding 10,000 km/sec. We have rederived distances and uncertainties to each of these clusters using the above-calibrated expression for the Tully-Fisher relation. The results are contained in Figure 9. A linear fit to the data in Figure 9 gives a Hubble constant of $H_o = 76$ km/sec/Mpc with a total observed scatter giving a formal (random) uncertainty on the mean of only ±2 km/sec/Mpc. It is significant that neither Fornax nor Virgo deviate to any significant degree from an inward extrapolation of this far-field solution. At face value, these results provide evidence for both of these clusters having only small motions with respect to their local Hubble flow. This value compares favorably with other recent calibrations of Tully-Fisher by Giovanelli *et al* (1997) who obtain $H_o = 69 \pm 5$ km/sec/Mpc (one sigma) and then by Tully (1998) who finds $H_o = 82 \pm 16$ km/sec/Mpc (95% confidence).

9. OTHER RELATIVE DISTANCE DETERMINATIONS

In addition to the relative distances using the Tully-Fisher relation discussed above, a set of relative distance moduli based on a number of independent secondary distance indicators, including brightest cluster galaxies, Tully-Fisher and supernovae is also available (Jerjen & Tammann 1993). We adopt, without modification, their differential distance scale and tie into the Cepheid distance to the Fornax cluster, which was part of their cluster sample. The results are shown in Figure 10 which extends the velocity-distance relation out to more than 160 Mpc. No error bars are given in the published compilation. For a discussion of uncertainties in this sample see Huchra (1995). This sample yields a value of $H_o = 72\ (\pm 1)_r$ km/sec/Mpc (random), with a systematic error of 10% being associated with the distance (but not the velocity) of the Fornax cluster.

10. BEYOND FORNAX: TYPE IA SUPERNOVAE

The Fornax cluster elliptical galaxies NGC 1316 and NGC 1380 are host to the well-observed type Ia supernovae 1980N and 1992A, respectively. The new Cepheid distance to NGC 1365, and associated estimate of the distance to the Fornax cluster thus allow two additional very high-quality objects to be added to the calibration of type Ia supernovae. A preliminary discussion of these objects was given by Freedman et al. (1997). Adding the Fornax supernovae to the type Ia supernovae sample of Sandage et al. (1996), and applying this calibration to the distant Type Ia supernovae of Hamuy (1995) gives $H_0 = 67$ km/sec/Mpc. In this analysis, low weight is given to historical supernovae (1895B, 1937C and 1960F) observed photographically. In addition, we have included a decline-rate absolute-magnitude relation (Phillips 1993; Hamuy et al. 1995; Reiss, Press & Kirshner 1996). Eliminating the new Fornax calibrators from the analysis changes the Hubble constant by -3 km/sec/Mpc.

11. COMPARING AND COMBINING THE RESULTS

The results of the previous five sections are presented in Table 3. What is the summary conclusion? In the first instance we can simply state that H_o falls within the full-range extremes of $67(\pm7)_r$ and $76(\pm2)_r$ km/sec/Mpc, with no obvious dependence on the indicative volume of space being probed. Hence, a variety of independent distance determination methods are yielding agreement at the 10% level. With the exception of the common Cepheid PL relation zero point, these various determinations are largely independent; thus their differences are indicative of the true systematic errors affecting each of the methods and their individual underlying assumptions. No single determination stands out as either markedly anomalous or as undeniably superior.

How then do we combine these individual results in a summary number with its own uncertainty? We have undertaken two types of approach: a *Frequentist* approach and a *Bayesian* one. In the end they only differ in their resulting confidence intervals. We begin by first considering the random errors.

In our application of the Frequentist approach (*e.g.,* Wall 1997 and references therein) we simply represent each determination as a probability distribution having its mean at H(i), a dispersion of $\sigma(\mathrm{i})_{\mathrm{random}}$ and unit integral (*i.e.,* equal total weight in the sum). These are shown as the connected dotted lines in the left panel of Figure 11; where, for instance, the low-dispersion solution of $72(\pm1)_r$ km/sec/Mpc based on the hybrid methods of Jerjen & Tammann (1993) peaking up at the center of the distribution. The solid enveloping line is the resulting sum of the five probability density distributions. The composite probability distribution is highly non-Gaussian, but it is still centrally peaked with both the mode and the median coinciding at 72 km/sec/Mpc. An estimate of the traditional (±one-sigma) errors can be easily obtained from this distribution by identifying where the cumulative probability hits 0.16 and 0.84, respectively. This procedure gives the cited ±5 km/sec/Mpc.

The Bayesian estimate is equally straightforward (see Press 1997). Again, taking the individual

Hubble constant estimates to be represented by Gaussians we combine them by multiplication, assuming a minimum-bias (flat) prior (Sivia 1996). We note that the Bayesian approach assumes statistical independence; and strictly speaking the considered samples are not completely independent given that they explicitly share a common (Cepheid) zero point, and the Jerjen & Tammann hybrid sample overlaps in part with the pure Tully-Fisher application. Nevertheless we have done the exercise of computing the posterior probability distribution with these caveats clearly stated. Because of the strong overlap in the various estimates the combined solution is both very strongly peaked and symmetric giving a value of $H_o = 72.6(\pm 0.8)_r$ km/sec/Mpc as depicted in the right panel of Figure 11. The one-sigma error on the mean was again determined from the 0.16 and 0.84 cumulative probability points. As already anticipated above the results of the two analyses are indistinguishable except for the high confidence attributed to the number by the Bayesian analysis. These results are summarized graphically in Figure 11 and numerically in Table 3.

Systematic errors must be dealt with separately and independently from the random error discussion. While some of the identified systematic errors affect all of the above determinations equally and in the same sense (the LMC distance modulus for instance), others are more 'randomly' distributed among the methods and their contributing galaxies. For instance, the (as yet unknown) effects of flows are estimated and scaled for each of the methods here, but they may be large for the Fornax cluster, but smaller and perhaps have a different sign for the ensemble of type Ia supernovae. It seems prudent therefore to simply average the systematic errors while listing out the main components individually. They are: (1) Large scale flow fields, contributing large fractional uncertainties to the nearest estimate of H_o, but dropping to only a few percent at large distances and/or for samples averaged over many directions (see Table 2 and further discussion below). (2) The zero point of the adopted PL relation, which in our case is tied directly to the adopted true distance modulus of the LMC. A variety of independent estimates are reviewed by Westerlund (1996) and he concludes that the uncertainty is at the 5% level in distance. And finally (3) the

metallicity dependence of the Cepheid PL relation. This is a complex and much debated topic and the interested reader is referred to Sasselov et al (1997), Kochanek (1997), Kennicutt et al. (1998), and earlier reviews by Freedman & Madore (1990) for an introduction to the literature. The metallicity of the galaxies for which Cepheid searches have been undertaken span a range in [O/H] abundance of almost an order of magnitude, with a median value of -0.3 dex. The calibrating LMC has a very similar abundance of [O/H] = -0.4 dex. These results suggest that even if in individual cases the metallicity effect amounted to 10-20%, the overall effect on the calibration of secondary distance indicators will be less than 5-10%. Upcoming observations with NICMOS on HST should further help to constrain the magnitude of this effect.

The importance of bulk flow motions on the determination of H_0 varies significantly depending on how far a particular distance indicator can be extended to (see Table 2). For local distance indicators the uncertainties due to unknown bulk motions are the largest contributing source of systematic error to the determination of H_o, amounting to an uncertainty of 20-25% in the local value of the Hubble constant. The Tully-Fisher relation extends to a velocity distance of about 10,000 km/sec, although most of the observed clusters are not this remote. At 6,000 km/sec, peculiar motions of ~300 km/sec would individually contribute 5% perturbations; however, with many clusters distributed over the sky, peculiar motions of this magnitude will give only a few percent uncertainty. For type Ia supernovae which extend to beyond 30,000 km/sec, the problem is even less severe. These estimates are consistent with recent studies by Shi & Turner (1998) and Zehavi et al. (1998) which place limits on the variation of H_o with distance, based on theoretical and empirical considerations, respectively.

13. COSMOLOGICAL IMPLICATIONS

A value of the Hubble constant, in combination with an independent estimate of the average density of the Universe, can be used to estimate a dynamical age for the Universe (*e.g.*, see Figure 12). For a value of of $H_o = 72\ (\pm 5)_r$ km/sec/Mpc, the age ranges from a high of ~12 Gyr for

a low-density ($\Omega = 0.2$) Universe, to a young age of $\sim$9 Gyr for a critical-density ($\Omega = 1.0$) Universe. These ages change to 15 and 7.5 Gyr, respectively allowing for an error of $\pm$10 km/sec/Mpc.

The ages of Galactic globular clusters traditionally are thought to fall in the range of 14$\pm$2 Gyr (Chaboyer, Demarque, Kernan & Krauss 1996); however, the subdwarf parallaxes obtained by the Hipparcos satellite (Reid 1997) may reduce these ages considerably. For $\tau = 14$ Gyr and $\Omega = 1.0$, H_o would have to be $\sim$45 km/sec/Mpc; interpreted within the context of the standard Einstein-de Sitter model, our value of $H_o = 72$ km/sec/Mpc, is incompatible with a high-density ($\Omega = 1.0$) model universe without a cosmological constant (at the 2-sigma level defined by the identified systematic errors.) If, however, $\tau = 11$ Gyr, then the globular cluster and the expansion ages are consistent to within their mutually quoted uncertainties.

Acknowledgements

This research was supported by the National Aeronautics and Space Administration (NASA) and the National Science Foundation (NSF), and benefited from the use of the NASA/IPAC Extragalactic Database (NED). Observations are based on data obtained using the *Hubble Space Telescope* which is operated by the Space Telescope Science Institute under contract from the Association of Universities for Research in Astronomy. LF acknowledges support by NASA through Hubble Fellowship grant HF-01081.01-96A awarded by the Space Telescope Science Institute, which is operated by the Association of Universities for Research in Astronomy, Inc., for NASA under contract NAS 5-26555

REFERENCES

Aaronson, M., Mould, J., Huchra, J., Sullivan, W. T., Schommer, R. A., & Bothun, G. D. 1980, ApJ, 239, 12

Bureau, M., Mould, J. R., & Staveley-Smith, L. 1996 ApJ, 463, 60, 1996

Chaboyer, B., Demarque, P., Kernan, P. J., & Krauss, L. M. 1996, Science, 271, 957

Coles, P., & Lucchin, F., 1995, in *Cosmology,* Wiley, 399

de Vaucouleurs, G., 1975 in *Stars and Stellar Systems,* **9**, eds. A. R. Sandage, M. Sandage, J. Kristian, Univ Chicago Press: Chicago, p. 557

Drinkwater, M. J., & Gregg, M. D. 1998, MNRAS, (submitted) = astro/ph9801016

Feast, M. W., & Catchpole, R. M. 1997, MNRAS, 286, L1

Ferguson, H. C. 1989, AJ, 98, 367

Ferguson, H. C., & Sandage, A. R. 1988, AJ, 96, 1520

Ferrarese, L. et al. 1996, ApJ, 464, 568

Freedman, W. L. 1990, ApJL, 355, L35

Freedman, W. L., & Madore, B. F. 1990, ApJ, 365, 186

Freedman, W. L., Madore, B. F. & Kennicutt, R. 1997, in *The Extragalactic Distance Scale*, eds. M. Livio, M. Donahue & N. Panagia, Cambridge Univ. Press: Cambridge, 171

Freedman, W. L., et al. 1994a, ApJ, 435, L31

Freedman, W. L., et al. 1994b, Nature, 371, 757,

Freedman, W. L., et al. 1998, in preparation

Giovanelli, R., Haynes, M. P., Da Costa, L. N., Freudling, W., Salzer, J. J., & Wegner, G. 1997, ApJ, 477, L1

Graham, J. A., et al. 1997, ApJ, 477, 535

Hamuy, M., et al. 1995, AJ, 109, 1

Han, M. S. 1992, ApJS, 81, 35

Han M., & Mould, J. R. 1990, ApJ, 360, 448

Hill, R., et al. 1998, ApJS, in press

Holtzmann, J., et al. 1995, PASP, 107, 156

Hubble, E. P. 1929, Proc. Nat. Acad. Sci., 15, 168

Huchra, J., Geller, M., Clemens, C., Tokarz, S. & Michel, A. 1992, Bull. CDS, 41, 31.

Huchra, J. 1995, Heron Island Conference on *Peculiar Velocities in the Universe*, P. Quinn and W. Zurek, eds. (published on the World Wide Web at http://msowww.anu.edu.au/ heron).

Jacoby, G., et al. 1992, PASP, 104, 599

Jerjen, H., & Tammann, G. A. 1993, A&A, 276, 1

Kennicutt, R. C., Freedman, W. L., & Mould, J. R. 1995, AJ, 110, 1476

Kennicutt, R. C., et al. 1998, ApJ, in press

Kochanek, C. S. 1997, ApJ, 491, 13

Kraan-Korteweg, R. 1986, A&AS, 66, 255

Lafler, J., & Kinman, T. D. 1965, ApJS, 11, 216

Madore, B. F., Freedman, W. L. & Sakai, S. 1997, in *The Extragalactic Distance Scale*, eds. M. Livio, M. Donahue & N. Panagia, Cambridge Univ. Press: Cambridge, 239

Madore, B. F., et al. 1998, Nature, submitted

Madore, B. F., & Freedman, W. L. 1991, PASP, 103, 933

Madore, B. F., & Freedman, W. L. 1998, ApJ, 491, in press

Mathewson, D. S., Ford, V. L., & Buchhorn, M. 1992, ApJS, 81, 413

Mould, J. R., Sakai, S., Hughes, S., & Han, M. 1997, in *The Extragalactic Distance Scale*, eds. M. Livio, M. Donahue & N. Panagia, Cambridge Univ. Press: Cambridge, 158

Mould, J. R., et al. 1995, ApJ, 449, 413

Phelps, R., et al. 1998, ApJ, submitted

Pierce, M. 1994, ApJ, 430, 53

Press, W. 1997, in *Unsolved Problems in Astrophysics*, eds J.P. Ostriker & J.N. Bahcall, Princeton Univ. Press: Princeton, p.49

Rawson, D. M., et al. 1997, ApJ, 490, 517

Reid, N. AJ, 114, 161, 1997

Riess, A. C., Press, W. H. & Kirschner, R. P. 1996, ApJ, 473, 88

Saha, A., Sandage, A. R., Labhardt, L., Tammann, G. A., Macchetto, F. D., & Panagia, N. 1996, ApJ, 466, 55

Sandage, A. R., Saha, A., Tammann, G. A., Labhardt, L., Panagia, N., & Macchetto, F. D. 1996, ApJL, 460, L15

Sasselov, D. D., et al. 1997, A&A, 324, 471

Schechter, P. 1980, AJ, 85, 801

Schechter, P., Mateo, M. Saha, A. 1993, PASP, 105, 1342

Schroder, A. 1995, Doctoral Thesis, University of Basel

Shi, X., & Turner, M. 1998, ApJ, 493, 519

Silbermann, N. A., et al. 1996, ApJ, 470, 1

Silbermann, N. A., et al. 1998, ApJ, submitted

Sivia, D. S., 1996, Data Analysis: A Bayesian Tutorial, Claredon Press: Oxford

Stetson, P. B. 1994, PASP, 106, 250 ,

Tammann, G. A. & Federspiel, M. 1997, in *The Extragalactic Distance Scale*, eds. M. Livio, M. Donahue & N. Panagia, Cambridge Univ. Press: Cambridge, 137

Tully, R. B. 1998, in *Cosmological Parameters of the Universe*, IAU Symp. 183, ed. K. Sato, Reidel: Dordrecht, (in press)

Wall, J. V. 1997, QJRAS, 37, 519

Westerlund, B. 1996, in *The Magellanic Clouds,* Cambridge Univ. Press: Cambridge

Zehavi, I, Reiss, A., Kirshner, R. P., & Dekel, A. 1998, ApJ submitted astrop-ph 9802252

FIGURE CAPTIONS

Fig. 1. – A comparison of the distribution of galaxies as projected on the sky for the Virgo cluster (right panel) and the Fornax cluster (left panel). M100 and NGC 1365 are each individually marked by arrows showing their relative disposition with respect to the main body and cores of their respective clusters. Units are arcmin.

Fig. 2. – Fornax galaxies with published radial velocities within 6° of the cluster center and having apparent velocities less than 2,500 km/sec. All 111 galaxies used to define the mean velocity (and velocity dispersion) for the Fornax cluster are shown plotted as they appear on the sky. The 71 early-type galaxies are depicted by filled circles; the 40 late-type galaxies are show as open circles. NGC 1365, near the center of the cluster, is individually marked.

Fig. 3. – Velocity-position plots for 111 Fornax galaxies. The right-hand portion of the figure shows the galaxies projected in declination down onto a right ascension slice of the sky. NGC 1365 is marked, and seen to be centrally located in both position ans velocity. Open circles are spiral/irregular galaxies; filled circles represent E/S0 galaxies.

Fig. 4. – The velocity structure of the Fornax cluster. The upper left insert shows that simple binned histogram of the 111 velocities for galaxies in the Fornax cluster. The distribution is symmetric about 1,400 km/sec and is closely approximated by a Gaussian with a one-sigma width of ~340 km/sec. Another representation of the velocity density distribution is given in the main portion of the left panel. Here we have represented each galaxy as an individual Gaussian of unit weight centered at its quoted velocity and widened by its published uncertainty (tall spikes represent high-precision velocities; low, broad smears represent uncertain observations). The solid curve is the sum of the individual Gaussians.

To obtain a mean and sigma from this probabilistic distribution we refer to the right panel where the cumulative probability density (CPD) distribution is plotted. Horizontal lines at CPD =

0.50, 0.16 and 0.84 cross the distribution curve at the mean velocity and at ±one-sigma, respectively. These are to be compared to the simple average and standard deviation shown by the centrally plotted error bar. The close coincidence of the two estimates is a direct reflection of the highly Gaussian nature of the Fornax velocity distribution. At the based of each of the plots the velocity of NGC 1365 is shown, fitting well within the one-sigma velocity dispersion.

Fig. 5. – V and I-band Period-Luminosity relations for the 37 Cepheids discovered in NGC 1365. The fits are to the fiducial relations given by (Madore & Freedman 1991) shifted to the apparent distance modulus of NGC 1365. Dashed lines indicate the expected intrinsic (2-sigma) width of the relationship due to the finite temperature width of the Cepheid instability strip. The solid line is a minimum χ^2 fit to the fiducial PL relation for LMC Cepheids (18), corrected for $E(B-V)_{LMC} = 0.10$ mag, scaled to an LMC true distance modulus of $\mu_o = 18.50$ mag, and shifted into registration with the Fornax data. [Note: Recent results from the Hipparcos satellite bearing on the Galactic calibration of the Cepheid zero point (Feast & Catchpole 1997; Madore& Freedman 1998) indicate that the LMC calibration is confirmed at the level of uncertainty indicated in Table 1, with the possibility that a small (upward) correction to the LMC reddening may be indicated.]

Fig. 6. – Relative geometry (left panel), and the corresponding velocity vectors (right panel) for the disposition and flow of Fornax and the Local Group with respect to the Virgo cluster. The circles plotted at the positions of the Virgo and Fornax clusters have the same angular size as the circles enclosing M100 and NGC 1365 in the two panels of Figure 1.

Fig. 7. – The velocity-distance relation for local galaxies having Cepheid-based distances. Circled dots mark the velocities and distances of the parent groups or clusters. The one-sided "error" bars with galaxy names attached mark the velocities associated with the individual galaxies having direct Cepheid distances. The heavy broken line represents a fit to the data giving $H_o = 73(\pm 4)_r$ km/sec/Mpc. The observed scatter is ±12 km/sec/Mpc, and is shown by the thin diverging broken lines.

Fig. 8. – Tully-Fisher relations. The left panel shows the absolute I-band magnitude, M_I versus the inclination-corrected 21-cm line widths for galaxies having individually determined Cepheid distances. NGC 1365 is the brightest object in this sample; the position of this *cluster spiral* is consistent with an extrapolation of the relation defined by the lower luminosity *field galaxy sample.* The right panel shows the calibrating sample (filled circles) superimposed on the entire population of Fornax spiral galaxies for which I-band observations and line widths are available; the latter being shifted to absolute magnitudes by the Cepheid distance to NGC 1365.

Fig. 9. – The velocity–distance relation for 16 clusters of galaxies out to 11,000 km/sec, having distance moduli determined from the I-band Tully-Fisher relation. A fit to the data gives a Hubble constant of $H_o = 76(\pm 2)_r$ km/sec/Mpc. The solid lines mark one-sigma bounds on the observed internal scatter.

Fig. 10. – The velocity–distance relation for 17 clusters of galaxies, having published (Jerjen & Tammann 1993) differential distance moduli scaled to the Fornax cluster. A fit to the data gives a Hubble constant of $H_o = 72(\pm 1)_r$ km/sec/Mpc. As in Figure 7, the solid lines mark one-sigma bounds on the observed internal scatter.

Fig. 11. – A graphical representation of Table 3 is given in the left panel, showing the various determinations of the Hubble constant, and the adopted mean. Each value of H_o and its statistical uncertainty is represented by a Gaussian of unit area (linked dotted line) centered on its determined value and having a dispersion equal to the quoted *random* error. Superposed immediately above each Gaussian is a horizontal bar representing the one sigma limits of the calculated *systematic errors* derived for that determination. The adopted average value and its probability distribution function (continuous solid line) is the arithmetic sum of the individual Gaussians. (This Frequentist representation treats each determination as independent, and assumes no *a priori* reason to prefer one solution over another.) A Bayesian representation of the products of the various probability density distributions is shown in the right panel. Because of the close proximity and strong overlap

in the various independent solutions the Bayesian estimator is very similar to, while more sharply defined than, the Frequentist solution.

Fig. 12. – Lines of fixed time representing the theoretical ages of the oldest globular cluster stars are shown for 12, 14 and 16 Gyr, plotted as a function of the expansion rate H_o and density parameter Ω_o, for an Einstein-de Sitter universe with the cosmological constant $\Lambda = 0$. The thick dashed horizontal line at $H = 72\ (\pm 5)_r\ [\pm 12]_s$ km/sec/Mpc is the average value of the Hubble constant given in Table 3. The parallel (solid) lines on either side of that solution represent the one-sigma random errors on that solution. Systematic errors on the solution for H_0 are represented by thin dashed lines at 61 and 83 km/sec/Mpc. The only region of (marginal) overlap between these two constraints is in the low density ($\Omega < 0.2$) regime, unless $\Lambda \neq 0$. If the globular cluster ages are assumed to place *a lower bound* on the age of the Universe, the region of plausible overlap between the two solutions is more severely restricted to even lower density models.

TABLE 1

ERROR BUDGET THE CEPHEID DISTANCE TO NGC1365

Source of Uncertainty on the Mean	Description of Uncertainty	Percentage Error	
LMC	**CEPHEID PL CALIBRATION**		
[A] **LMC True Modulus**	Independent Estimates = 18.50 ±0.10 mag	5%	
[B] **V PL Zero Point**	LMC PL $\sigma_V = (0.27)/\sqrt{31} = \pm 0.05$ mag	3%	
[C] **I PL Zero Point**	LMC PL $\sigma_I = (0.18)/\sqrt{31} = \pm 0.03$ mag	2%	
[SC] **Systematic Uncertainty**	[A] + [B] + [C] combined in quadrature		6%
NGC 1365	**CEPHEID TRUE DISTANCE MODULUS**		
(D) **HST V-Band Zero Point**	On-Orbit Calibration: ±0.05 mag	3%	
(E) **HST I-Band Zero Point**	On-Orbit Calibration: ±0.05 mag	3%	
(M1) **Cepheid True Modulus**	(D)(E) are uncorrelated, but coupled by reddening law: $\sigma_{\mu_o} = \pm 0.15$ mag	7%	
(F) **Cepheid V Modulus**	NGC 1365 PL $\sigma_V = (0.32)/\sqrt{37} = \pm 0.05$ mag	3%	
(G) **Cepheid I Modulus**	NGC 1365 PL $\sigma_I = (0.31)/\sqrt{37} = \pm 0.05$ mag	3%	
(M2) **Cepheid True Modulus**	(F)(G) are partially correlated, giving $\sigma_{\mu_o} = \pm 0.06$ mag	3%	
(P1) **V-Band Ap. Corr.**	Silberman *et al.* (1998) give ±0.067 mag	3%	
(P2) **I-Band Ap. Corr.**	Silberman *et al.* (1998) give ±0.061 mag	3%	
(M3) **Cepheid True Modulus**	(P1)(P2) are uncorrelated, but coupled by reddening law: $\sigma_{\mu_o} = \pm 0.15$ mag	7%	
[Z] **Metallicity**	M31 metallicity gradient test gives $\sigma_{\mu_o} = \pm 0.08$ mag	4%	
	M101 calibration gives +0.14 mag of $\Delta\mu_o/\Delta[Fe/H] = -0.25$ mag/dex	7%	
[H] **Reduction Package**	Systematic differences in aperture corrections (achromatic)	4%	
(J) **Random Errors**	(M1) + (M2) + (M3) combined in quadrature		10%
[K] **Systematic Errors**	[SC] + [Z] + [H] combined in quadrature		10%
	D = 18.6 Mpc ± 1.9 (random) ± 1.9 [systematic]		

Note: There are 32 Cepheids in the LMC with published VI photometry (Madore & Freedman 1991.) The measured dispersions in the period-luminosity relations at V and I are ±0.27 and ±0.18 mag, respectively.

TABLE 2

ERROR BUDGET ON THE HUBBLE CONSTANT

Source of Uncertainty on the Mean	Description of Uncertainty	Percentage Error	
FORNAX CLUSTER	**EXPANSION VELOCITY AND INFERRED DISTANCE**		
(L) **Velocity Dispersion**	± 31 km/sec $= \pm 342/\sqrt{N-1}$ (No. of gals = 117) at $< V >=$ 1,306 km/sec	2%	
(M) **Geometry of Cluster**	± 0.4 Mpc at 18.6 Mpc	2%	
[N] **Virgocentric Flow**	± 22 km/sec on -44 km/sec along the Local Group line of sight	2%	
[O1] **Bulk Flow**	± 300 km/sec	24%	
Random Errors	(J) + (L) + (M) combined in quadrature		10%
Systematic Errors	[K] + [N] + [O1] combined in quadrature		26%
	$H_o = 70$ km/sec/Mpc $\pm$ 7 (random) ± 18 [systematic]		
LOCAL FLOW	**M81, M101, N1023, N2090, N3621, N7331, LEO, VIRGO, FORNAX**		
(P) **Random Motions**	± 4 km/sec/Mpc $= \pm 12/\sqrt{N-1}$ (No. of samples = 9)	6%	
[O2] **Bulk Flow**	± 300 km/sec at $V(max) = +1{,}400$ km/sec	21%	
Random Errors	(P) = total observed scatter on the mean		6%
Systematic Errors	[SC] + [Z] + [O2] combined in quadrature		23%
	$H_o = 73$ km/sec/Mpc $\pm$ 4 (random) $\pm$ 17 [systematic]		
DISTANT FLOW	**I. TULLY-FISHER: 16 CLUSTERS TO 10,000 km/sec**		
(S) **Observed Scatter**	$\pm$ 0.04 mag $= \pm$ 0.16/$\sqrt{N-1}$ (No. of clusters = 16)	2%	
[R] **TF Zero Point**	$\sigma(mean) = \pm$ 0.13 mag $= \pm$ 0.40/$\sqrt{N-1}$ (No. of calibrators = 11)	6%	
[O3] **Bulk Flow**	± 300 km/sec evaluated at 10,000 km/sec	3%	
Random Errors	(S)		2%
Systematic Errors	[SC] + [Z] + [R] + [O3] combined in quadrature		11%
	$H_o = 76$ km/sec/Mpc $\pm$ 2 (random) $\pm$ 8 [systematic]		
DISTANT FLOW	**II. HYBRID METHODS: 17 CLUSTERS TO 11,000 km/sec**		
(U) **Observed Scatter**	± 0.02 mag $= \pm 0.06/\sqrt{N-1}$ (No. of clusters = 17)	2%	
[O4] **Bulk Flow**	± 300 km/sec evaluated at 11,000 km/sec	3%	
[T] **Fornax Distance**	[SC] + [Z] combined in quadrature	9%	
Random Errors	(U)		2%
Systematic Errors	[T] + [Z] combined in quadrature		10%
	$H_o = 72$ km/sec/Mpc $\pm$ 1 (random) $\pm$ 7 [systematic]		
DISTANT FLOW	**III. Type Ia SN: 20 EVENTS OUT TO 20,000 km/sec**		
(T1) **Peak Luminosity**	± 0.11 mag $= \pm 0.45/\sqrt{N-1}$ (No. of SNIa = 16)	6%	
(V1) **Random Motions**	± 300 km/sec at 5,000 km/sec	6%	
[O5] **Bulk Flow**	± 300 km/sec at 20,000 km/sec	2%	
[Q1] **SNIa Zero Point**	$\sigma(mean) = \pm 0.18$ mag $= \pm 0.45/\sqrt{N-1}$ (No. of calibrators = 7)	9%	
Random Errors	(T1) + (V1) combined in quadrature		8%
Systematic Errors	[SC] + [O5] + [Q1] combined in quadrature		12%
	$H_o = 67$ km/sec/Mpc $\pm$ 5 (random) $\pm$ 8 [systematic]		

TABLE 3

SUMMARY

Method	Hubble Constant	(Random)	[Systematic]
Fornax Cluster	70 km/sec/Mpc	±7 (random)	±18 [systematic]
Local Flow	73 km/sec/Mpc	±4 (random)	±17 [systematic]
Tully-Fisher	76 km/sec/Mpc	±2 (random)	± 8 [systematic]
Hybrid Methods	72 km/sec/Mpc	±1 (random)	± 7 [systematic]
Type Ia SNe	67 km/sec/Mpc	±5 (random)	± 8 [systematic]
Modal Average:	72 km/sec/Mpc	±5 (random)	±12 [systematic]
Major Systematics:	±11% [FLOWS]	±5% [LMC]	±4% [Fe/H]

Notes: (1) The measured scatter of the $N = 5$ tabulated values of the Hubble constant about the derived mean of 72 km/sec/Mpc is ±3.1 km/sec/Mpc; the formal error on the unweighted mean (due to random errors between methods) is then $3.1/\sqrt{N-1} = 1.6$ km/sec/Mpc.

(2) The systematic error due to large-scale flows is the average of the ±300 km/sec term on each of the five methods. (24%, 21%, 3%, 3% and 2%, respectively, as given in Table 2)

(3) Calculated for differences in the five Hubble constants with respect to the mean, and scaled to their externally quoted errors, the reduced $\chi^2 = 0.78$. This is only slightly smaller than expected by chance, and suggests that the random errors on the individually determined values of the Hubble constant are realistic.

(4) The concordance between the local and far-field values of the the Hubble constant argue that there is no large flow of the local supercluster with respect to the 20,000 km/sec volume probed by the SNe. At face value the differences in Hubble constants admit a local flow of ~100 km/sec. If so, the (averaged) systematic error due to large scale flow perturbations drops from a dominant 10% down to <3-4%, leaving the LMC distance as the leading source of systematic error on H_o.

(5) The systematic uncertainty due to metallicity is derived from the work on M31 (Freedman & Madore 1990) which reports a marginal detection of a dependence of Cepheid luminosities on metallicity, at the level of ~0.2 mag/dex. A similar test using Cepheids at various radii in M101 has been undertaken by the Key Project Team (Kennicutt, *et al. 1998), and gives a slightly larger dependence of ~0.25 mag/dex.*

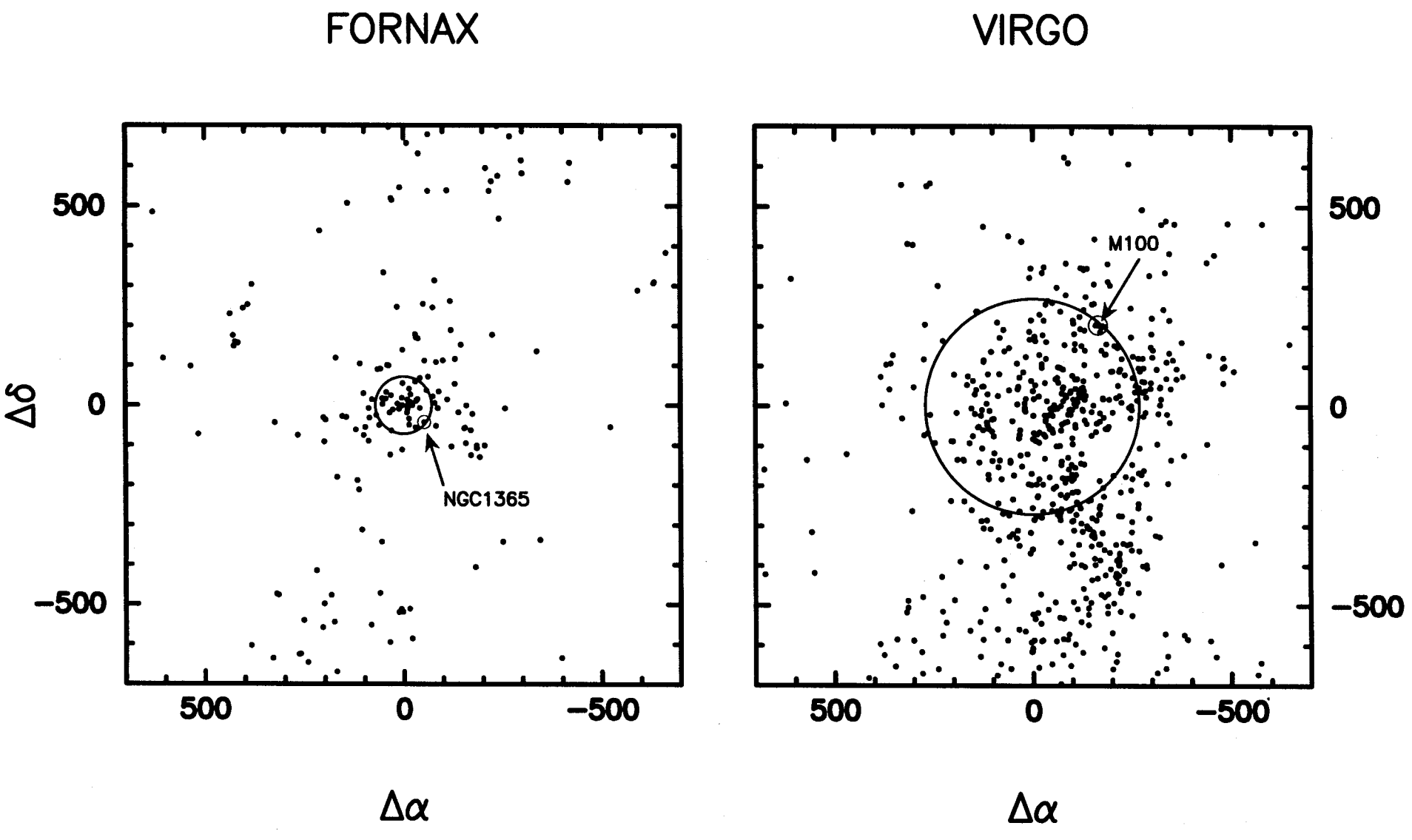
FORNAX
VIRGO
500
0
−500
Δδ
NGC1365
M100
500
0
−500
Δα
500
0
−500
Δα

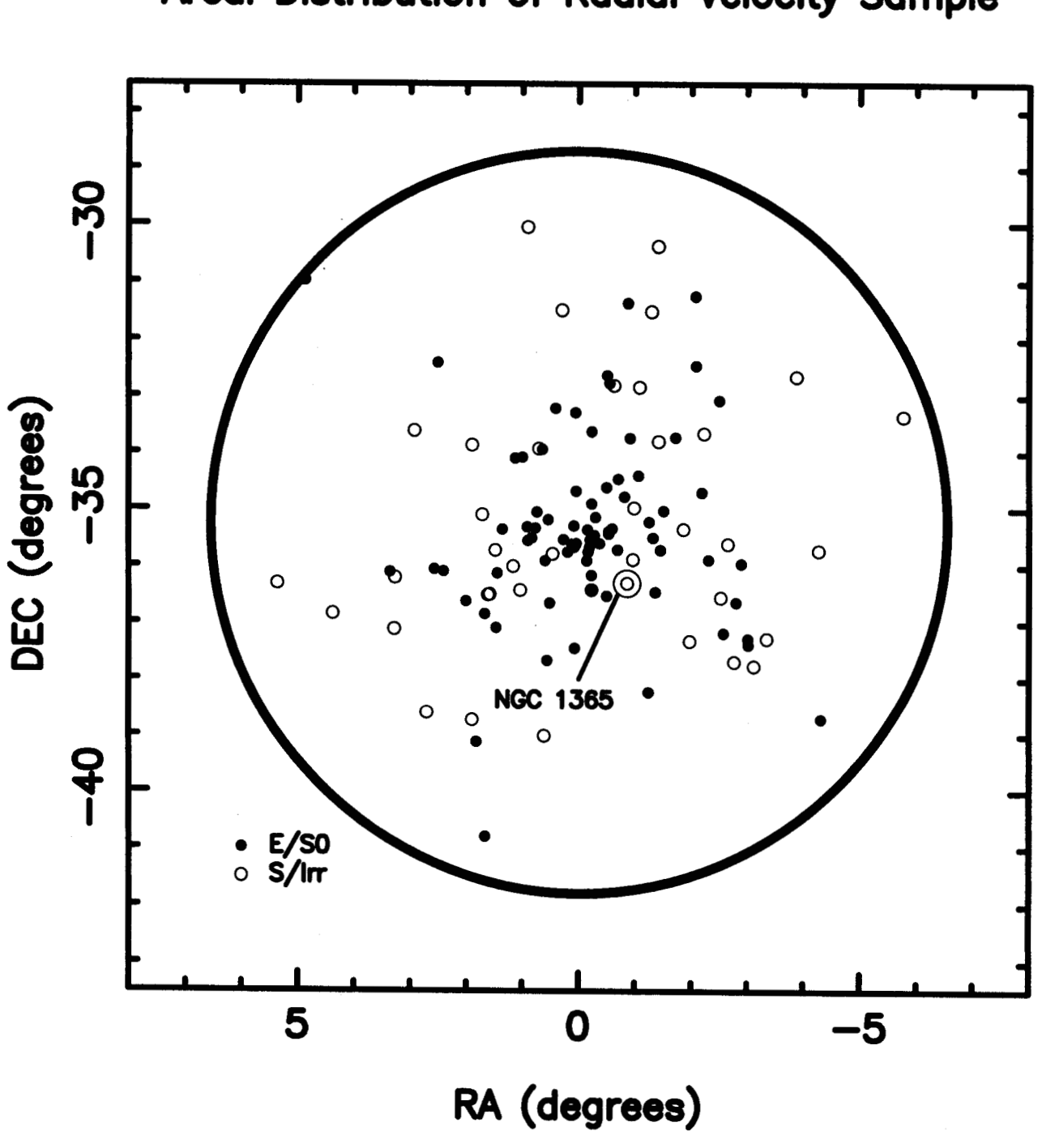
Areal Distribution of Radial Velocity Sample
DEC (degrees)
−30
−35
−40
NGC 1365
E/S0
S/Irr
5
0
−5
RA (degrees)

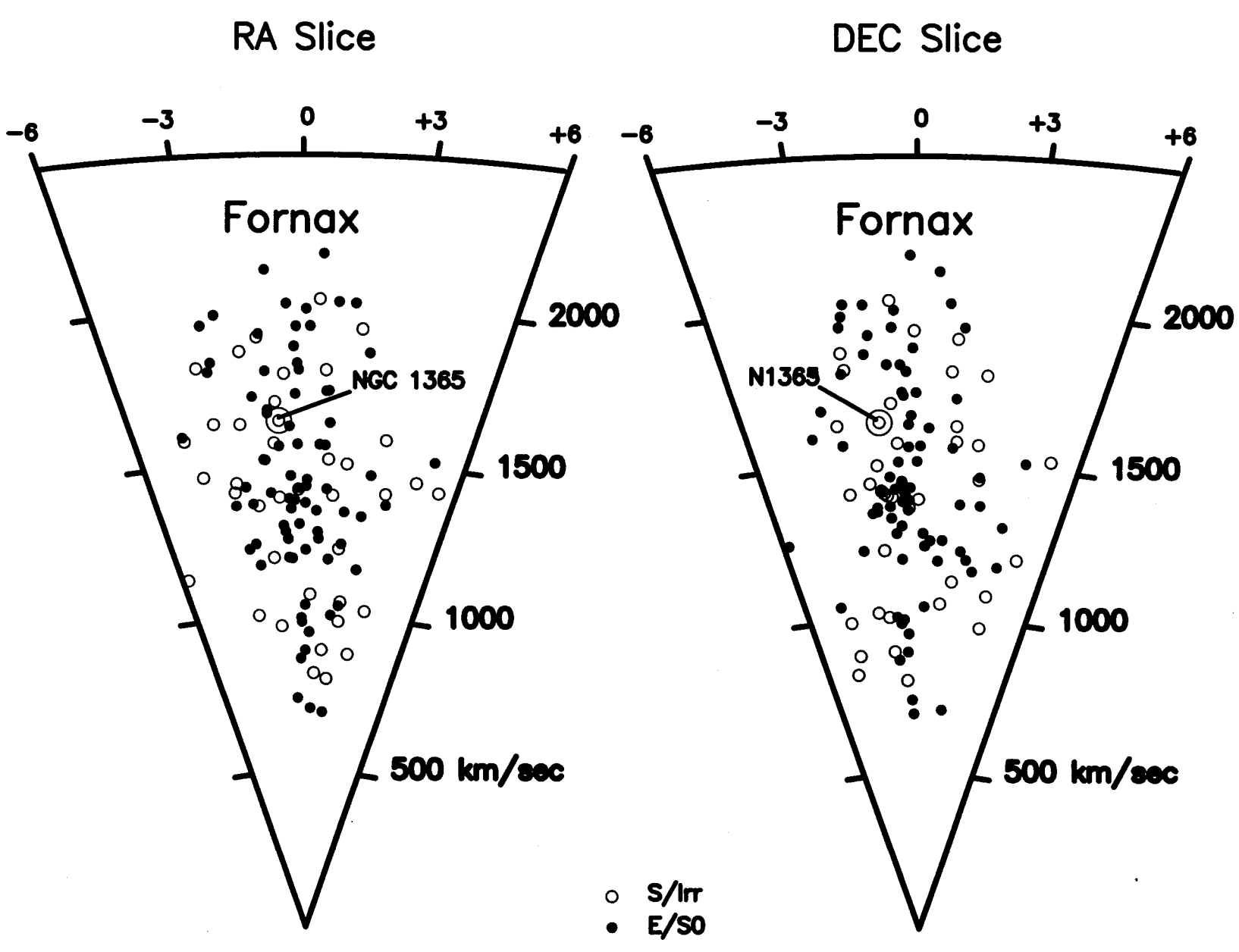
RA Slice
DEC Slice
-6
-3
0
+3
+6
Fornax
2000
1500
1000
500 km/sec
NGC 1365
N1365
S/Irr
E/S0

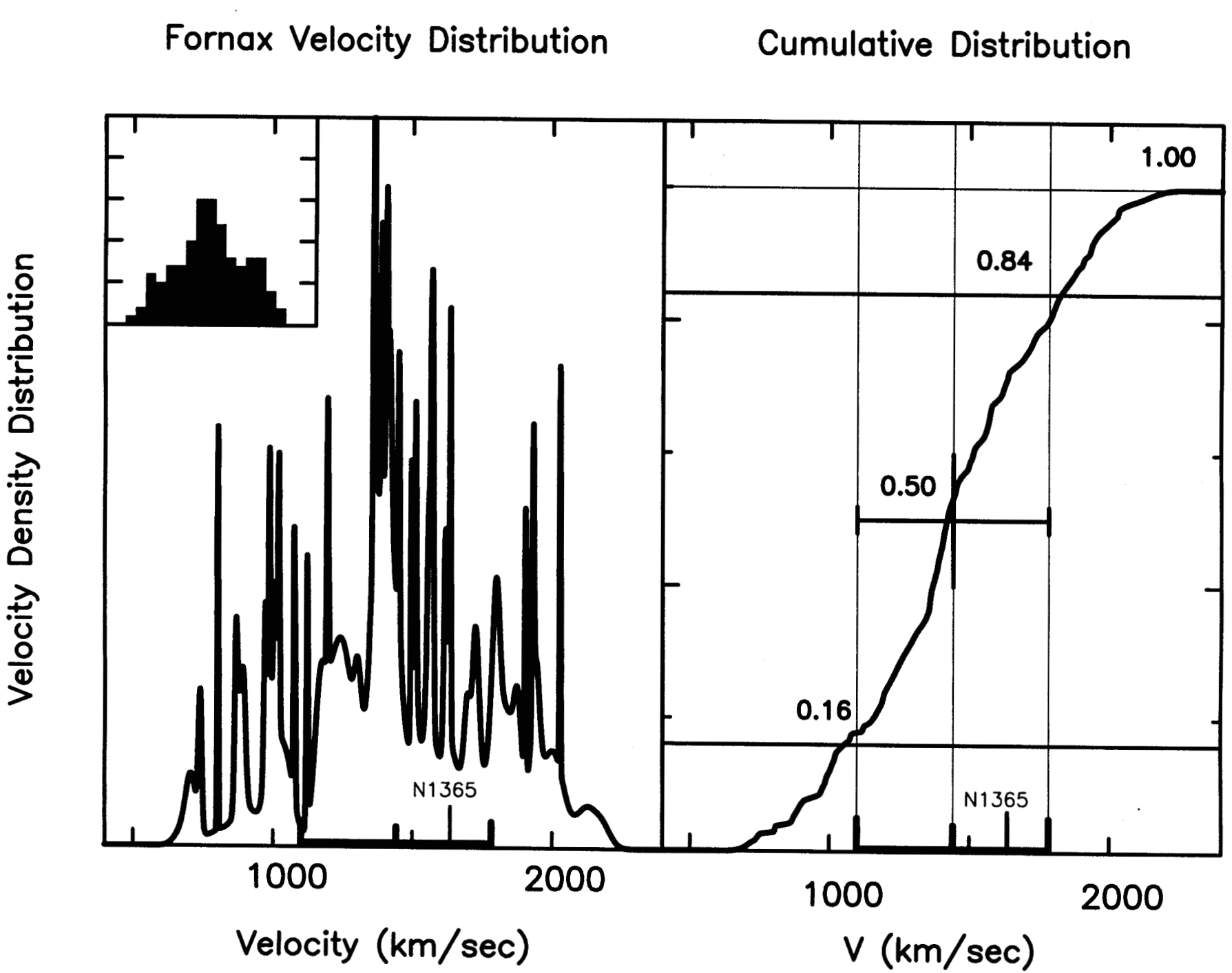
Fornax Velocity Distribution
Cumulative Distribution
Velocity Density Distribution
N1365
1000
2000
Velocity (km/sec)
1.00
0.84
0.50
0.16
N1365
1000
2000
V (km/sec)

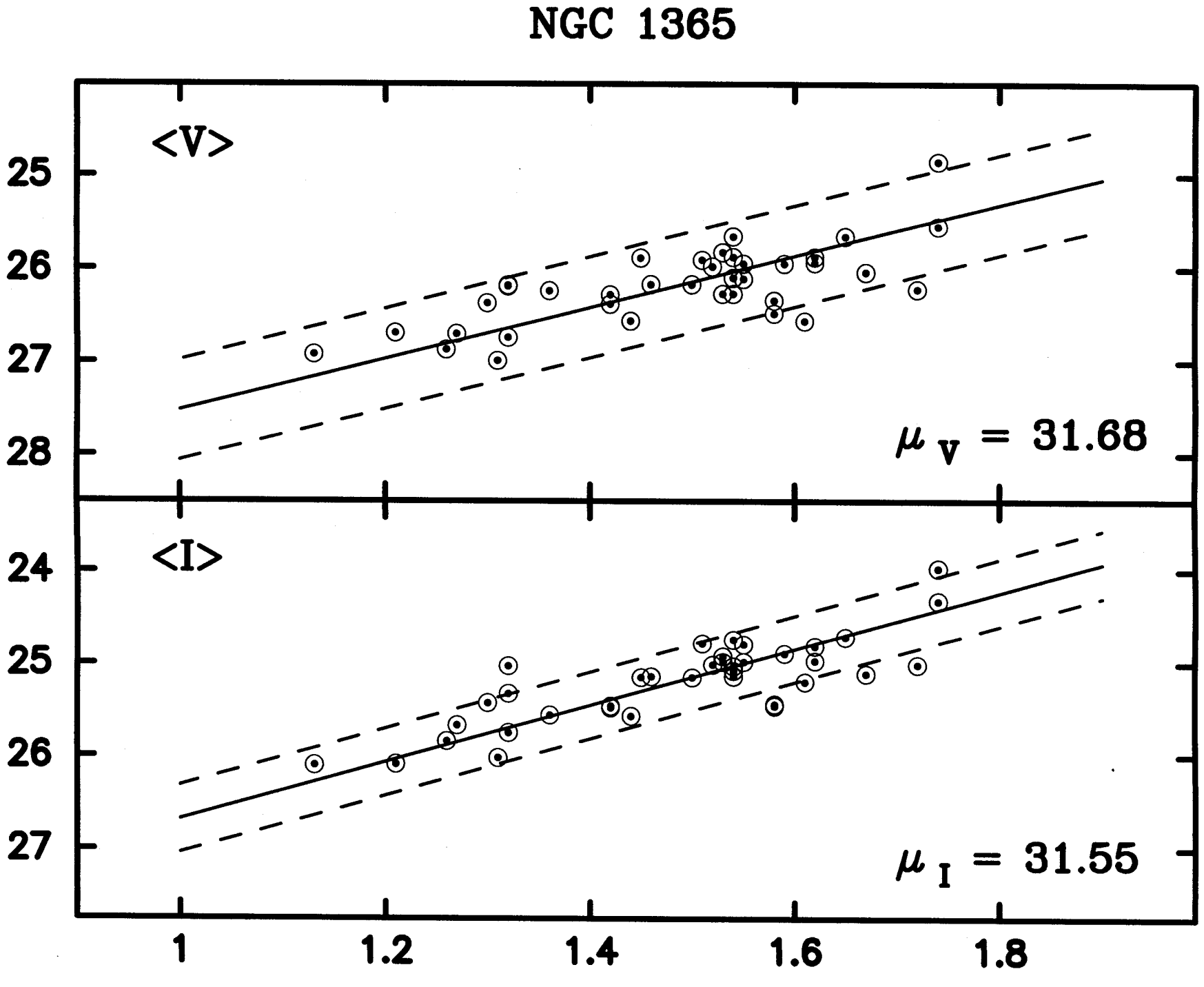
NGC 1365
<V>
25
26
27
28
$\mu_V = 31.68$
<I>
24
25
26
27
$\mu_I = 31.55$
1
1.2
1.4
1.6
1.8

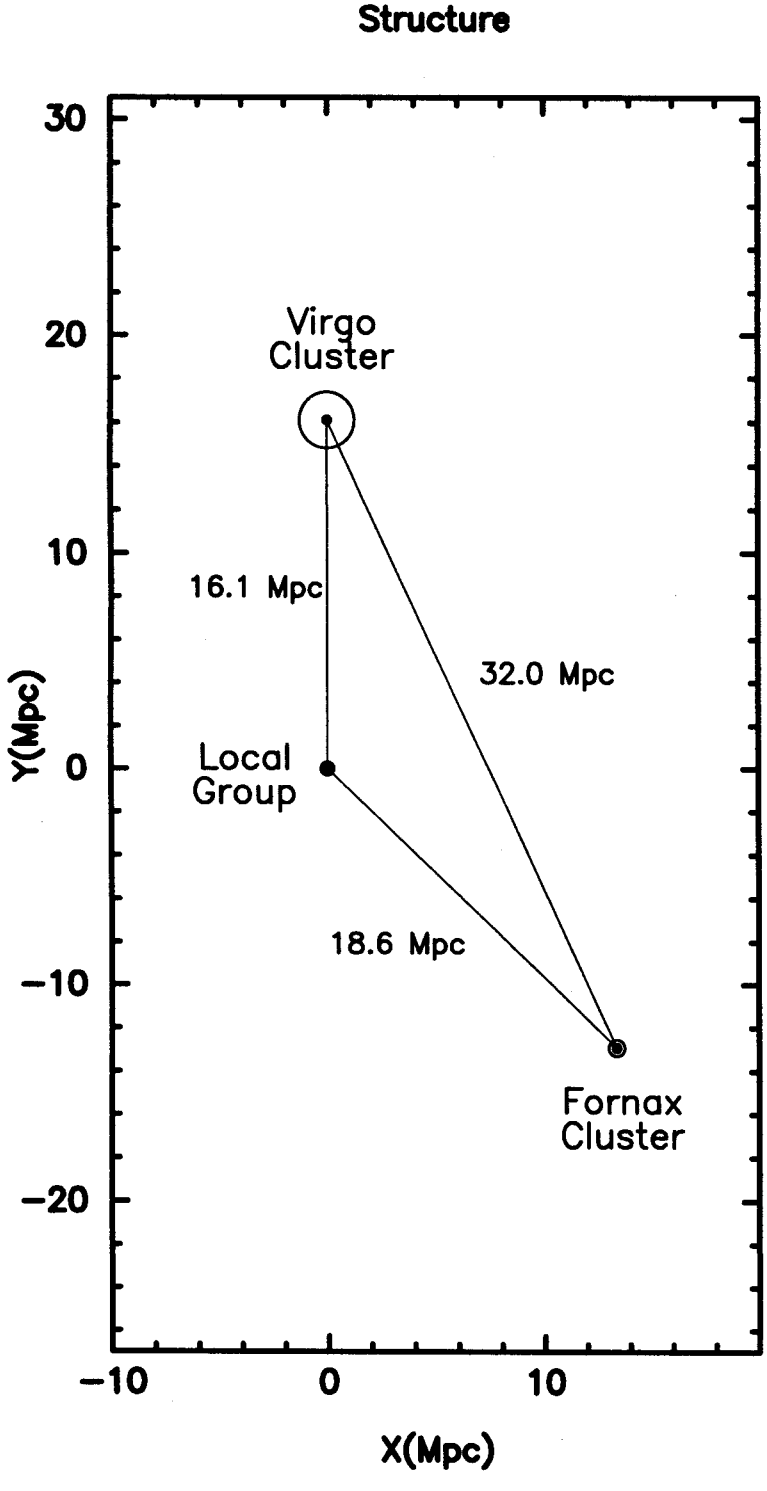
Structure
Virgo
Cluster
16.1 Mpc
32.0 Mpc
Local
Group
18.6 Mpc
Fornax
Cluster
Y(Mpc)
X(Mpc)
30
20
10
0
−10
−20
−10
0
10

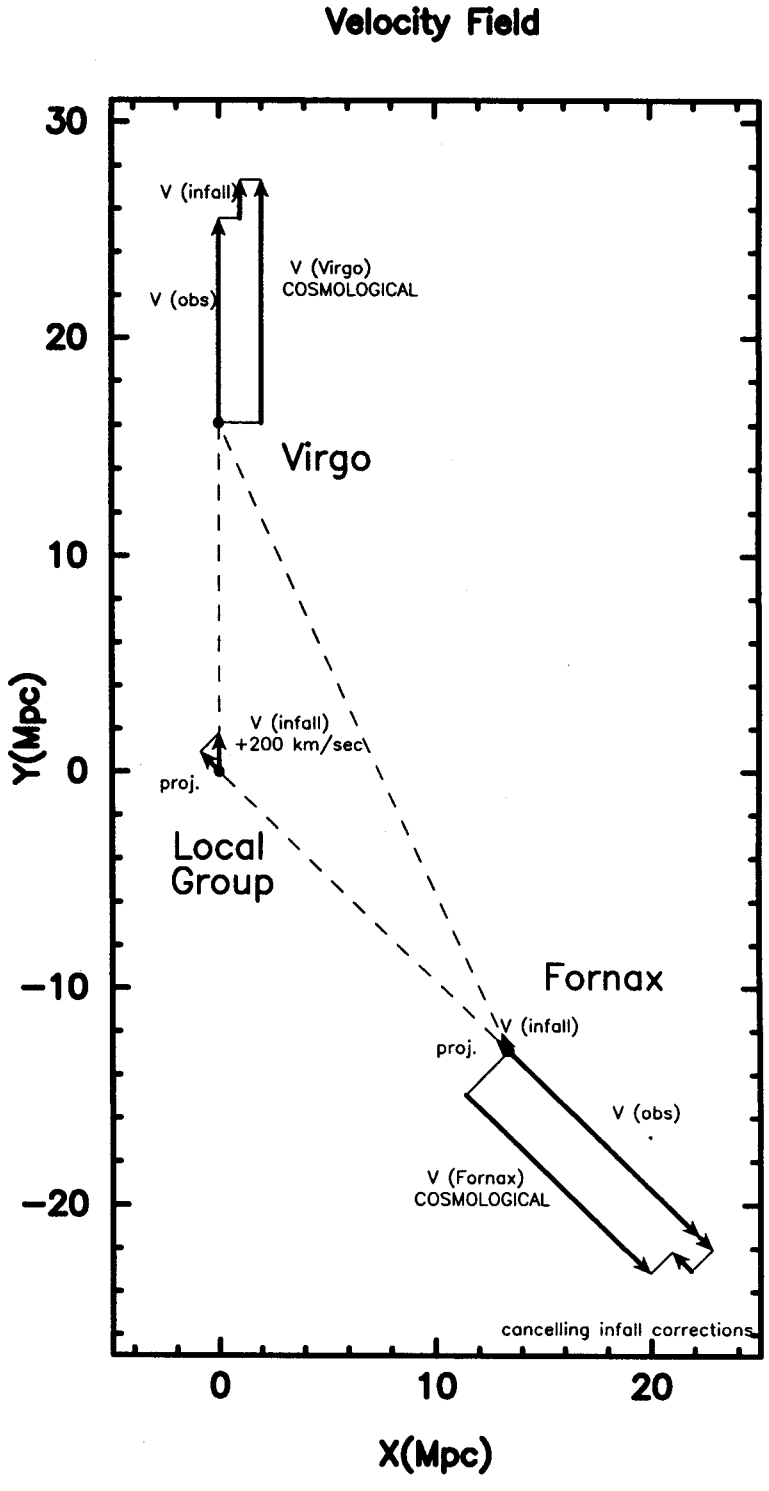
Velocity Field
V (infall)
V (obs)
V (Virgo)
COSMOLOGICAL
Virgo
V (infall)
+200 km/sec
proj.
Local
Group
Fornax
V (infall)
proj.
V (obs)
V (Fornax)
COSMOLOGICAL
cancelling infall corrections
Y(Mpc)
X(Mpc)
30
20
10
0
−10
−20
0
10
20

Local Hubble Constant

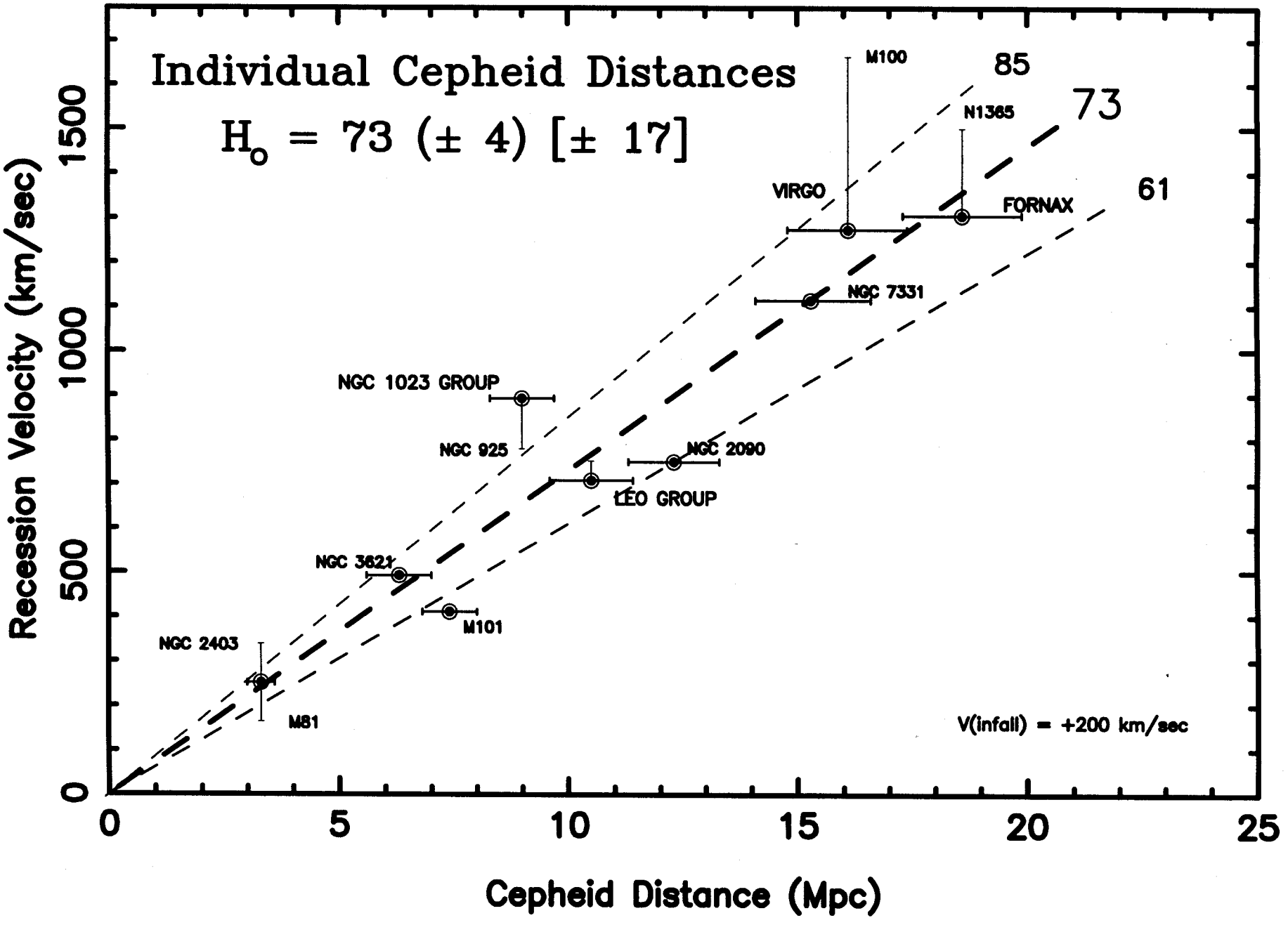

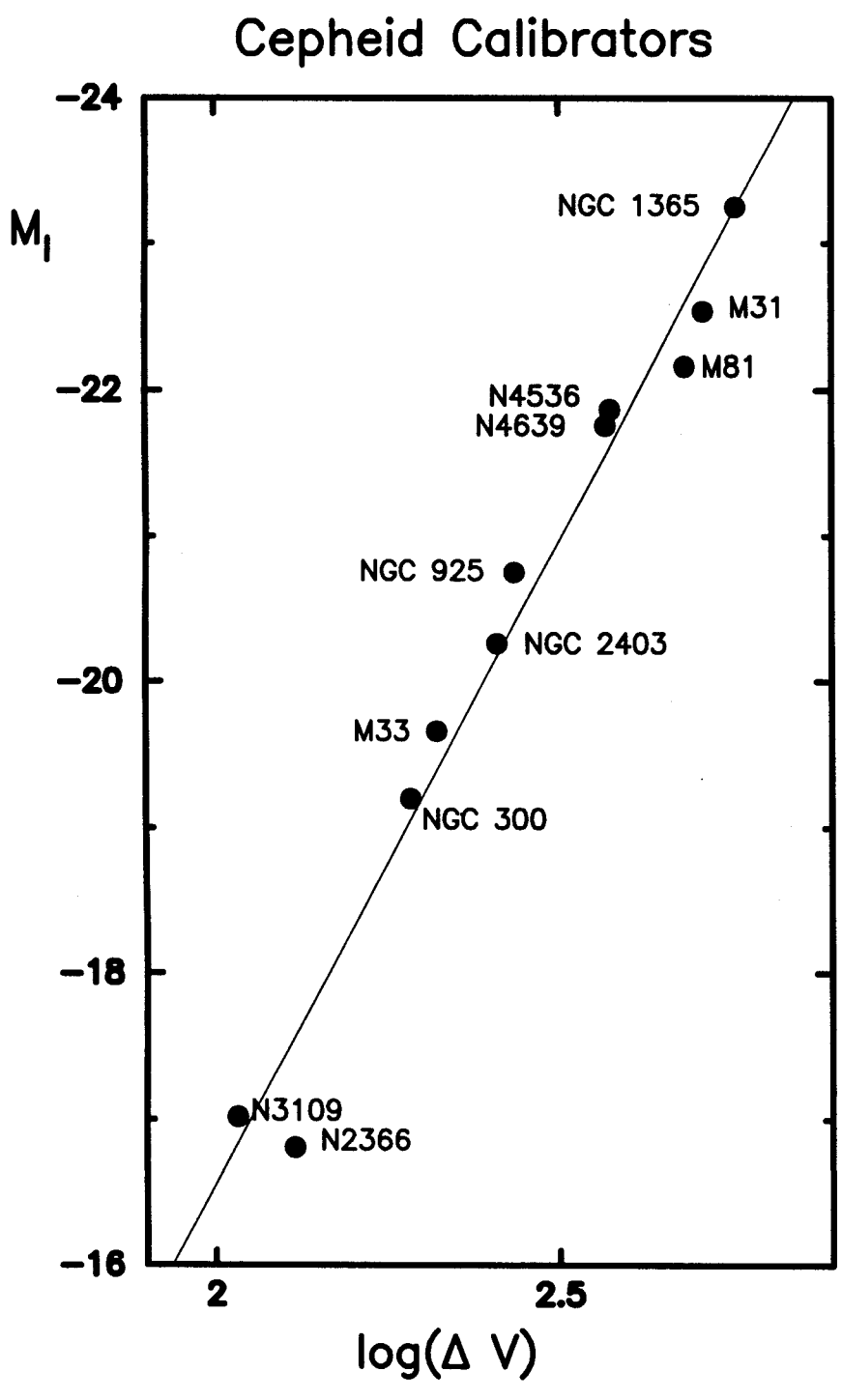
Cepheid Calibrators
M_I
−24
−22
−20
−18
−16
2
2.5
log(Δ V)
NGC 1365
M31
M81
N4536
N4639
NGC 925
NGC 2403
M33
NGC 300
N3109
N2366

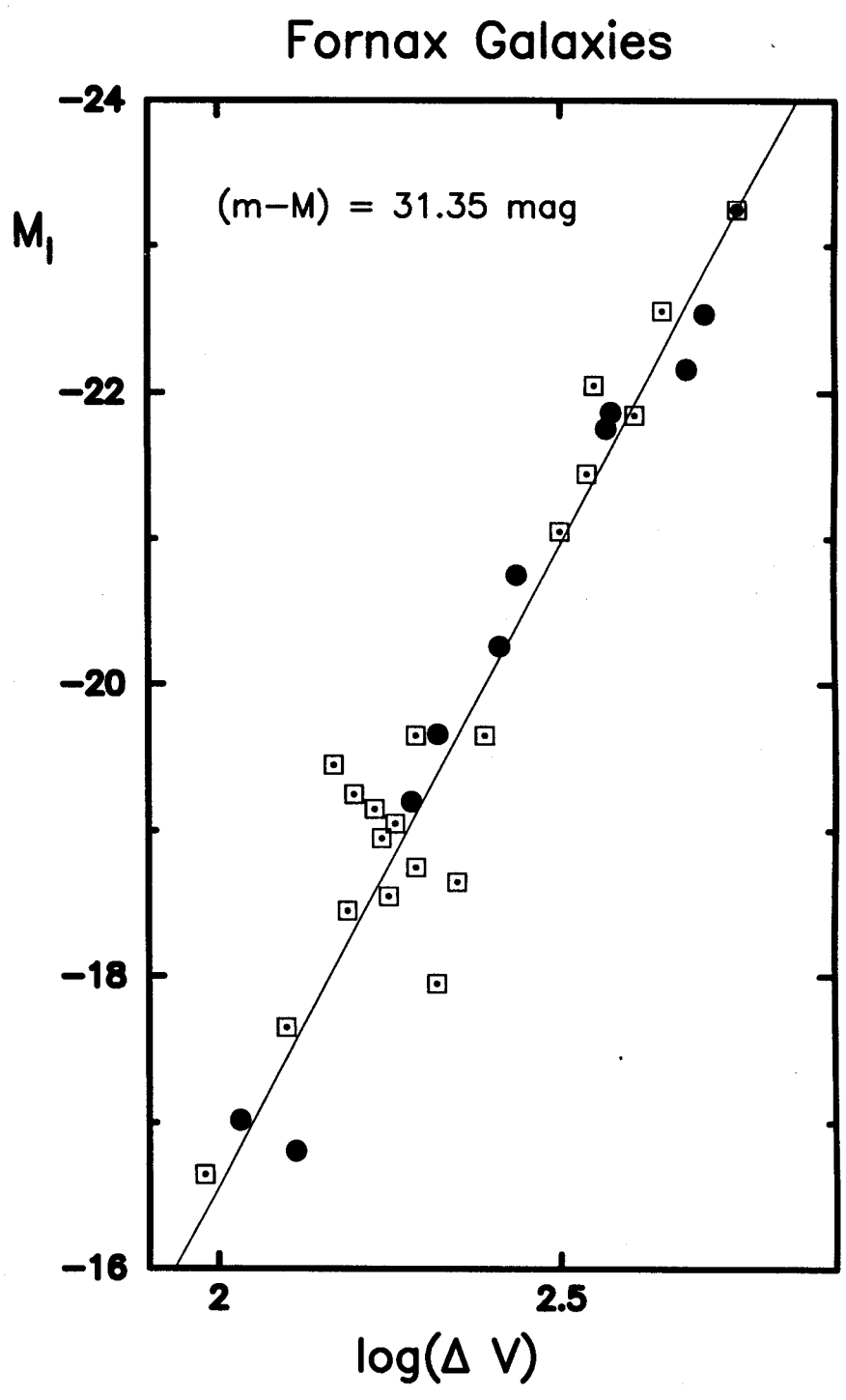
Fornax Galaxies
M_I
(m−M) = 31.35 mag
−24
−22
−20
−18
−16
2
2.5
log(Δ V)

Far–Field Hubble Constant

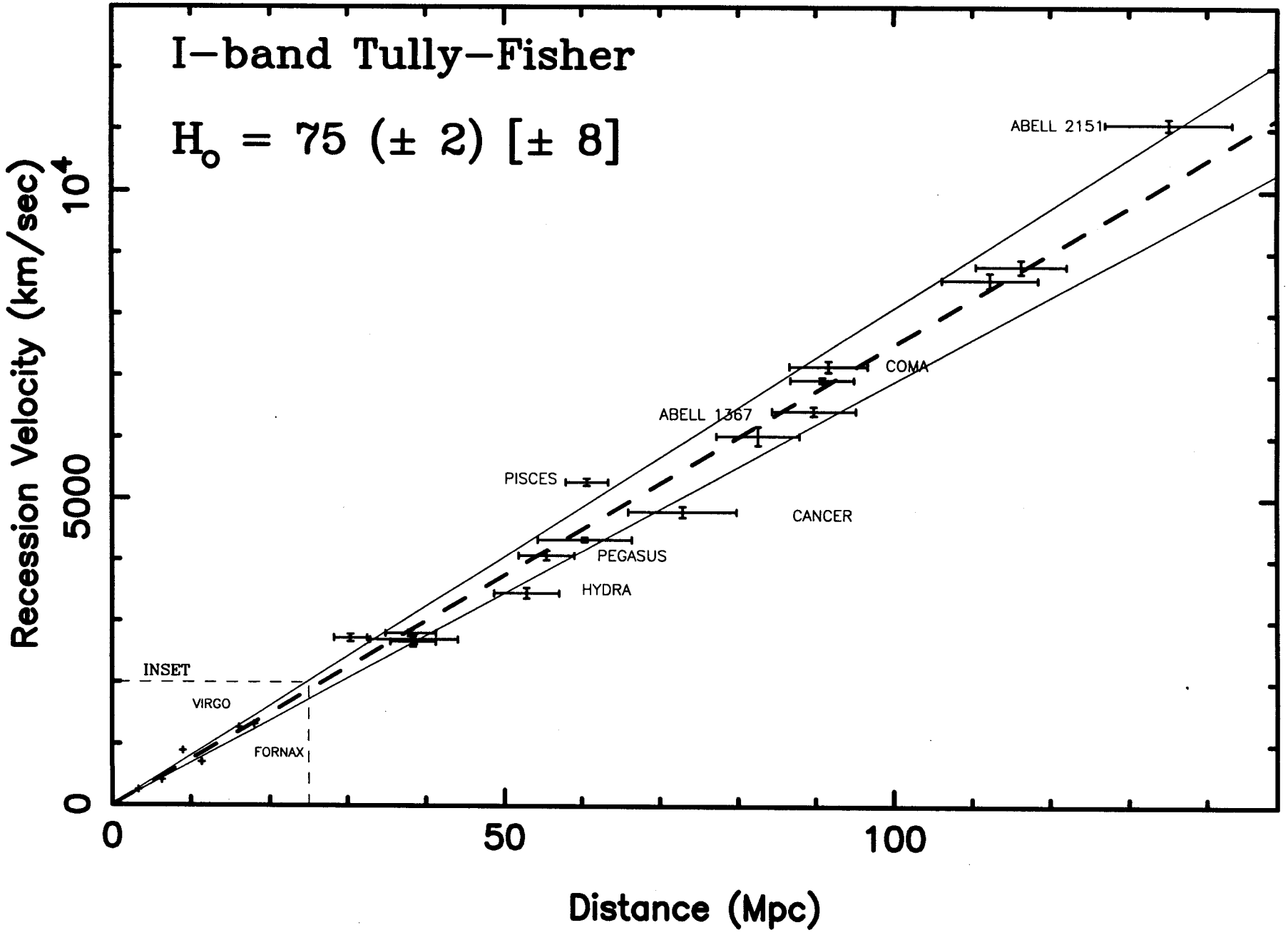

Hybrid Cluster Sample

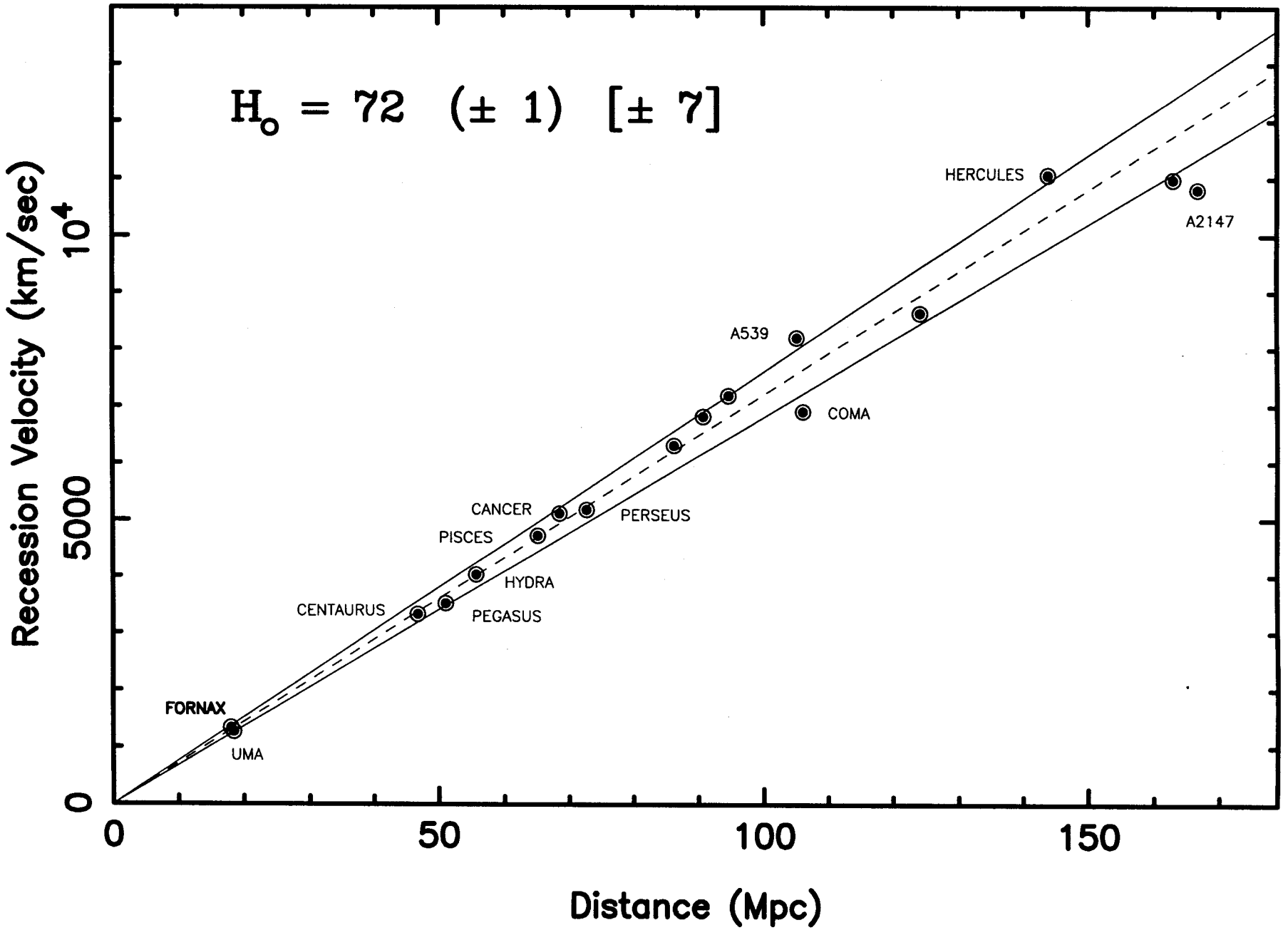

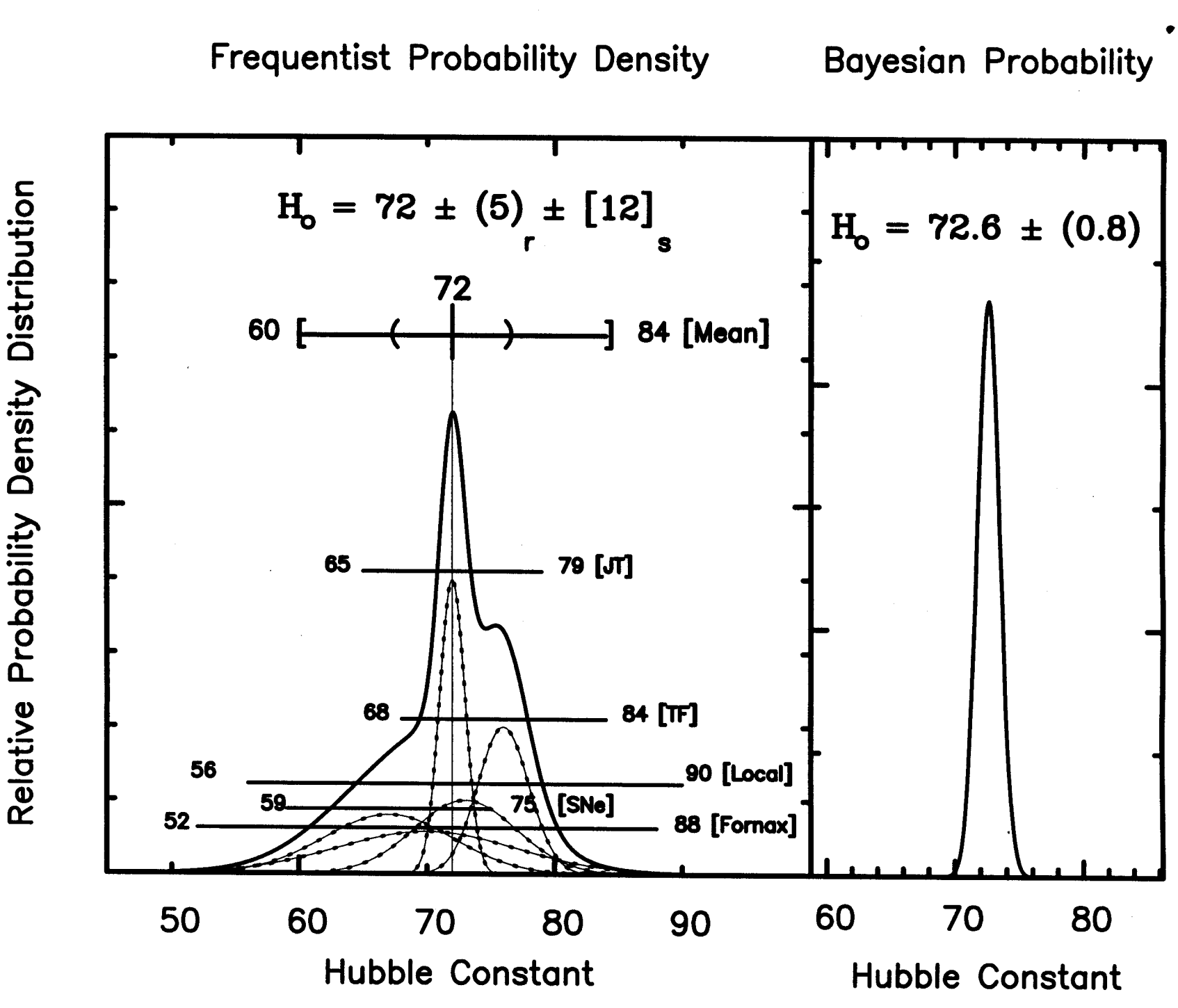
Frequentist Probability Density
Bayesian Probability
Relative Probability Density Distribution
$H_o = 72 \pm (5)_r \pm [12]_s$
72
60 [Mean] 84
65 [JT] 79
68 [TF] 84
56 [Local] 90
59 [SNe] 75
52 [Fornax] 88
$H_o = 72.6 \pm (0.8)$
50
60
70
80
90
60
70
80
Hubble Constant
Hubble Constant

Age Constraints